RSC Advances

ROYAL SOCIETY OF CHEMISTRY

www.rsc.org/advances

RSC Advances

PAPER

Hierarchically nanostructured hydroxyapatite microspheres as drug delivery carriers and their effects on cell viability

Received 00th January 20xx,
Accepted 00th January 20xx

DOI: 10.1039/x0xx00000x

www.rsc.org/

Haibo Duan,†[ab] Yijuan Ma,†[ab] Xiao Liu,[ab] Lijing Hao[ab] and Naru Zhao*[ab]

Hydroxyapatite microspheres (HAMSs) were fabricated via hydrothermal synthesis using propionamide (PA) as a pH-adjusting agent and trisodium citrate (TSC) as a regulating agent. Scanning electron microscope (SEM) images indicated that the microspheres possessed well-defined 3D nanostructures constructed by nanoplates as building blocks. *In vitro* cell tests demonstrated that the HAMSs with or without heat treatment were able to promote the proliferation of mouse bone mesenchymal stem cells (mBMSCs). Gentamicin sulphate (GS), an anti-inflammatory, was successfully loaded in the HAMS particles at a distinctively high loading efficiency of approximately 87%. The resultant HAMS-GS delivery systems displayed a sustained release property, and the release of GS from HAMS-B-GS500 system could significantly inhibit *S. epidermidis* growth. Moreover, the biocompatibility tests indicated that the HAMS-B-GS500 system exhibited excellent biocompatibility and had no toxic effects on the mBMSCs. These outstanding characteristics may make HAMSs a good candidate as an injectable and drug-loading biomaterial for *in vivo* tissue regeneration and drug control release.

1. Introduction

Hydroxyapatite (HA) is a major inorganic constituent of teeth and bones and has long been studied due to its excellent bioactivity, biocompatibility and osteoconductivity.[1-4] In recent years, HA-based drug carrier systems have been investigated for biomedical applications.[5-7] Previous studies have shown that the physicochemical properties of synthetic HA depend on its morphology, chemical composition and textural properties.[8,9] Among the different morphological and structural HA biomaterials, hierarchically nanostructured mesoporous HA materials exhibit high surface areas, large pore volumes and multiphase interfaces and able to efficiently adsorb biologically active species, especially drug molecules.[10,11] Additionally, HA microsphere materials have been shown to induce slight inflammation and contribute towards bone formation when compared with irregular particles.[12-14] When spherical granules of HA materials are uniformly packed, they could contribute to cell migration and extracellular matrix (ECM) growth through the vacancies formed between the spherical granules.[15]

Recently, various synthetic approaches have been proposed for the preparation of HA microspheres, including spray drying,[16,17] template method,[18] hydrothermal synthesis,[19,20] and emulsion technique.[21] Compared with other methods, the hydrothermal method has been shown to be a relatively simple and effective way to prepare well-crystallised HA microspheres by controlling, for example, the pH value, the hydrothermal temperature and the surfactant amount. However, hydrothermal synthesis of HA with regular morphology and good dispersion properties remains a significant challenge.

Highly ordered, complex architectures organised by nanostructured building blocks have potential applications in biomedical materials.[22] The use of surfactants and polymers has been demonstrated to modify mass transitions, provide nucleation sites, regulate the orientation of crystals and dominate the final morphology of crystals.[23] Many reports have shown that citrate can be used as a crystal modifier for HA crystallites and plays a vital role in regulating the final morphological and structural evolution of HA products from dumbbell-like to spherical particles.[24-27] Previous studies have shown that propionamide can improve the pH value of the synthesis solution by increasing hydrothermal temperature and time. The pH changes may lead to the gradual consumption of calcium and phosphate ions of the system, enabling the pre-formed HA crystal nuclei to continue growing in the supersaturated calcium and phosphate solution.[28] However, residual surfactants or introduced organic groups may deteriorate the bioactivity of biomaterials.[29,30] To maintain their bioactivity, the residual surfactants should be removed by calcination or other viable methods.

Implant-associated bacterial infections are grave complications that currently restrict the use of biomaterials in humans.[31,32] Conventional therapy with systemic antibiotics is often compromised due to poor accessibility to infection sites

[a] School of Materials Science and Engineering, South China University of Technology, Guangzhou 510641, China. E-mail: nrzhao@scut.edu.cn; Tel: +8620-87114645
[b] Nation Engineering Research Centre for Tissue Restoration and Reconstruction, Guangzhou 510006, China.
† These authors contributed equally to this work.

in bone tissues, particularly in necrotic or avascular tissues.[33] In recent years, local drug delivery systems in bone reconstruction have been adapted to obliterate the implant-associated infection. Conventional HA particles have limited drug loading capacities because of their low surface area. Moreover, drugs are released from conventional HA particles in a burst-release manner.[34] To overcome the aforementioned disadvantages, one strategy is to synthesize hierarchically nanostructured hydroxyapatite microspheres. The microspheres with well-defined 3D network structures and large surface areas make it possible to incorporate high doses of drugs and release them at controlled rates. Due to its low cost, broad antibacterial spectrum and good stability, gentamicin sulphate (GS) is extensively used as an antibiotic to prevent bone implant-associated infection.[35,36] Over 60% of chronic osteomyelitis cases were caused by *S. epidermidis*, which is sensitive to gentamicin.[37]

Herein, we demonstrated a facile hydrothermal method to prepare HA microspheres (HAMSs) constructed by nanoplates as building blocks using propionamide (PA) as a pH-adjusting agent and trisodium citrate (TSC) as a regulating agent. We investigated the effects of the HAMSs on the biocompatibility, drug delivery property and bactericidal property of GS-loaded HAMSs.

2. Materials and methods

2.1 Materials

Calcium nitrate (CN), ammonium phosphate ($(NH_4)_2HPO_4$), TSC and nitric acid (HNO_3) were purchased from Guangzhou Chemical Reagent Factory (Guangdong, China). PA and ammonia hydroxide (NH_4OH) were supplied by Aladdin (Shanghai, China). GS was purchased from Guangzhou Qiyun Biotechnology Co., Ltd. (Guangdong, China). All chemical reagents were of analytical grade without any further purification. Deionised water was obtained from a water purification system (Millipore S.A.S., France).

2.2 Preparation of HAMSs

HAMSs were prepared by a hydrothermal method using PA as a pH-adjusting agent and TSC as a regulating agent. According to previous reports,[38,39] stock solutions of Ca^{2+} and PO_4^{3-} were separately prepared by dissolving the desired amount of CN and $(NH_4)_2HPO_4$ in a 0.2 M HNO_3 solution. The Ca/P molar ratios were fixed at 1.67. TSC and PA were simultaneously added to the Ca^{2+} and PO_4^{3-} solutions, respectively. Then, the Ca^{2+} solution was added to the PO_4^{3-} solution under continuous stirring and the initial pH was adjusted to 3 using 2 M HNO_3 or 1:1 (v/v) ammonia. The adjusted solutions were transferred to a teflon-lined stainless steel autoclave. The autoclave was maintained at the 180 °C for 24 h and allowed to cool to room temperature. The products were separated by centrifugation at a rate of 4000 rpm for 5 min, washed five times with deionised water and lyophilised for two days. These samples were designated HAMS-B. A few of the samples were heat treated at 900 °C at a heating rate of 2 °C/min for 5 h; these samples were designated HAMS-HT.

2.3 Characterisation

The phase compositions of the as-synthesized products were characterised by powder X-ray diffraction (XRD, X'Pert PRO, PANalytical, Netherlands) with Cu Kα radiation (λ= 1.5418 Å). The chemical functional groups were investigated by Fourier transform infrared spectroscopy (FTIR, Vector 33, Bruker, Germany) within the wavenumber range of 4000-400 cm^{-1} using KBr as the standard. The morphology of the HA microspheres was observed using scanning electron microscopy (SEM, MERLIN Compact, Carl Zeiss, Germany). The samples were sputter-coated with gold to avoid charging under the electron beam prior to examination. The surface areas of samples were determined by the Brunauer-Emmett-Teller (BET) method using a surface area analyser (NOVA4200e, Quantachrome, USA). The samples were outgassed under vacuum for 12 h at 200 °C before the analysis. The pore size distribution and volumes were calculated from the adsorption branch using Barett–Joyner–Halenda (BJH) methods. The particle size distribution of samples was determined by Laser particle sizer (Mastersizer 2000, Malvern, England). The absorbance of gentamicin in the release media was measured using ultraviolet (UV) spectrophotometer (TU-1901, Beijing Purkinje General Instrument Co., Ltd., China).

2.4 Drug loading and *in vitro* drug release

The typical drug loading and *in vitro* drug release experiments were performed as follows: GS (200 or 500 mg) was added into 50 mL PBS (pH 7.40) with rapid stirring at a rate of 500 rpm to ensure an adequate dispersion. Then, 500 mg of samples were added into the solution. The vials were sealed to prevent the evaporation of PBS solution, and the mixture was stirred for 24 h at room temperature. Afterwards, the mixture was centrifuged at a rate of 4000 rpm for 5 min. The clear supernatant was then collected, and the GS amounts of clear supernatant were measured by UV spectrophotometer at 203 nm. At the same time, the GS-loaded HAMSs were dried in a vacuum oven at 50 °C until constant weight; the drug-loaded samples were named HAMS-GS200 and HAMS-GS500, respectively. The amount of GS encapsulated in the HAMSs was calculated by subtracting the amount of the GS in the supernatant (C_1) from the used GS amount (C_0). The loading amount of GS was determined by UV analysis by calculating the difference in the GS-PBS concentration before and after loading. The loading efficiency of GS (L. E.) was calculated according to the following equation:

$$\text{L. E.} = \frac{C_0 - C_1}{C_0} \times 100\%$$

For the *in vitro* drug release test, the GS-loaded HA microspheres (40 mg) were completely immersed in 50 mL of PBS solution at 37 °C under shaking at a constant rate of 160 rpm. The GS-release medium (3 mL) was collected for UV analysis at predetermined time intervals and replaced by the

same volume of fresh, 37 °C preheated PBS solution. The extracts were centrifuged at 4000 rpm for 5 min before measurement. All samples were subjected to drug release studies in triplicate.

2.5 Cell viability

Cytotoxicity tests were performed for HAMSs-treated mouse bone mesenchymal stem cells (mBMSCs) purchased from ATCC (ATCC CRL-12424) and cultured in Dulbecco's Modified Eagle's Medium (DMEM) supplemented with 10% foetal bovine serum (FBS). The cells were maintained at 37 °C in a moist environment with 5% CO_2. The cell suspensions (1×10^4 cells mL^{-1}) were seeded into 48-well plates with 500 µL per well and cultured for 24 h at 37 °C. After 24 h, the culture medium was refreshed with 500 µL culture medium containing samples at concentrations of 0, 100 and 200 µg mL^{-1}, followed by incubation for 1, 3 and 5 days. The HAMSs concentrations were determined after drying to constant weight, followed by heat sterilisation at 121 °C for 0.5 h, and UV sterilisation.

After 1, 3, and 5 days of culture, suspensions of HAMS particles were removed and washed with PBS. A mixture of 270 µL fresh culture medium and 30 µL CCK-8 solutions (Dojindo, Kumamoto, Japan) was added to each well. After incubation at 37 °C for 1 h, 100 µL supernatant was transferred into a 96-well plate and the absorbance was analysed at a wavelength of 450 nm using a microplate reader (Thermo 3001, Thermo Co., USA).

For cell viability evaluation, mBMSCs were plated in 48-well plates (Corning, NY, USA) and stained with Live/Dead stain kit (Dojindo, Kumamoto, Japan). Briefly, after 3 days of culture, the cells were washed three times with PBS and stained by mixture of calcein AM (2 µM) and PI (4 µM) for 30 min in the absence of light at 37 °C. Samples were washed twice times with PBS after staining and observed by the fluorescence microscopy (Eclipse Ti-U, Nikon, Japan).

2.6 Antibacterial activity

The *in vitro* antibacterial activity of the HAMS-B-GS500 system was quantitatively evaluated against *S. epidermidis* (ATCC 35984) by the standard plate count method.[40] Generally, *S. epidermidis* was grown in LB broth (1% w/v tryptone, 0.5% w/v yeast extract, 0.5% w/v NaCl) at 37 °C with 100 rpm agitation for 24 h, followed by centrifuging. The bacterial pellet was washed three times with deionised water, followed by resuspension in sterilised PBS solution. The concentrations of the prepared bacterial suspensions used for the antibacterial tests were 1×10^7 colony forming units (CFU) per mL. The HAMS-GS samples (2 mg) that had been immersed in PBS solution (2.5 mL) for 1, 3 and 5 days at 37 °C under shaking at a constant rate of 160 rpm were collected by centrifugation, gently washed three times with sterile PBS, and then resuspended in 100 µL sterilised PBS. Subsequently, the sample suspensions were transferred to 15 mL sterilised tubes and 900 µL of bacterial suspensions were added. After being incubated at 37 °C with shaking at 200 rpm for 6 h, the *S. epidermidis* in PBS was quantified by plating serial dilutions on agar plates. The agar plates were incubated for 24 h at 4 °C, and the total CFU were counted visually.

2.7 Statistical analysis

Results were represented as the means ± standard deviation (SD) and significant differences were assessed by Student's t-test. Differences were considered significant when $^*P < 0.05$, $^{**}P < 0.01$.

3. Results and discussion

3.1 Characterisation of HAMSs

Fig. 1 shows the morphology of the obtained samples (HAMS-B and HAMS-HT) as observed by SEM. Although both the HAMS-B and HAMS-HT samples exhibited a spherical shape with similar diameters in the range of 0.5-25 µm (Fig. 2), their morphologies and porous structures were different. The surfaces of the HAMS-B samples were observed to have numerous HA nano-needles, which were oriented normal to the surface, resulting in the formation of dandelion-like structures (Figs. 1a and c). Compared with the HAMS-B samples, numerous HA nanorods were distributed over the surfaces of the HAMS-HT samples. The nanorods interweaved to form porous structure (Figs. 1b and d). The EDS spectra indicated that the HAMSs samples mainly contained calcium (Ca), phosphorus (P), oxygen (O), and carbon (C). The Ca, P, O elements are derived from the HAMS, while the C elements may have originated from the conductive paste or the samples.

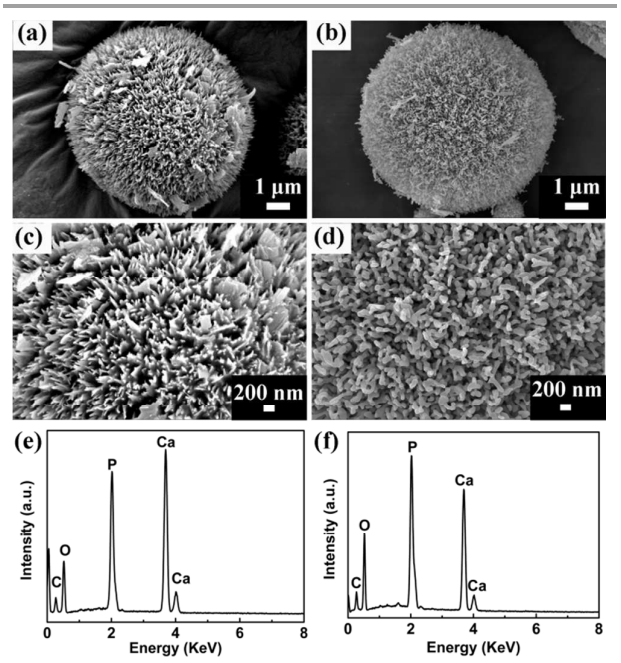

Fig. 1 SEM micrographs of samples: (a and c) HAMS-B; (b and d) HAMS-HT. EDS spectra of samples: (e) HAMS-B, (f) HAMS-HT.

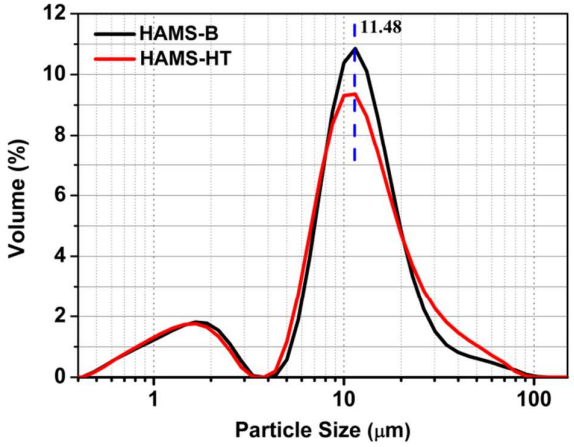

Fig. 2 Particle size distribution of HAMSs.

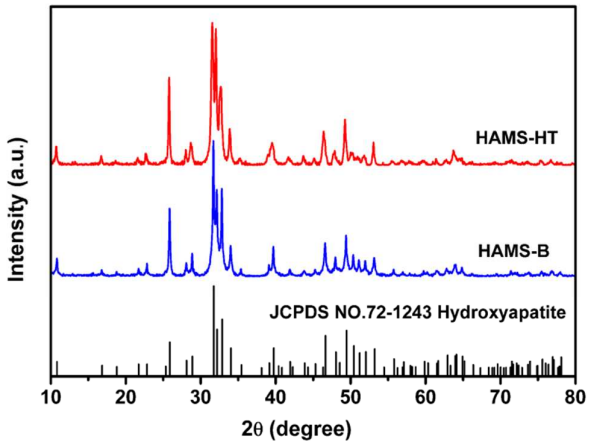

Fig. 3 XRD pattern of HAMSs.

The XRD patterns of the synthesised HAMSs (HAMS-B and HAMS-HT) in Fig. 3 indicated that the principal phase compositions of HAMS-B and HAMS-HT were identical. All diffraction peaks could be indexed as a single phase of HA (JCPDS No. 72-1243), and no peaks indicative of impurities were identified. The sharp peaks revealed that HA products were highly crystalline.

The FTIR spectra in Fig. 4 shows that the HAMS-B and HAMS-HT samples have similar composition and structure. The presence of carbonate bands at 1456, 1545 and 878 cm^{-1} were consistent with B- and A-type carbonate substituted HA, where carbonate ions replaced phosphate and hydroxyl groups in the crystal lattice, respectively.[41,42] Carbonate has been demonstrated as the prevalent anion substitution in biological apatite (approximately 4-8 wt.%), and their incorporation can improve the bioactivity and biodegradability of HA materials.[43-45] These results indicated that the prepared HAMSs were similar to the inorganic minerals of natural bone in the chemical components.

The porous structure of the HAMSs (HAMS-B and HAMS-HT)

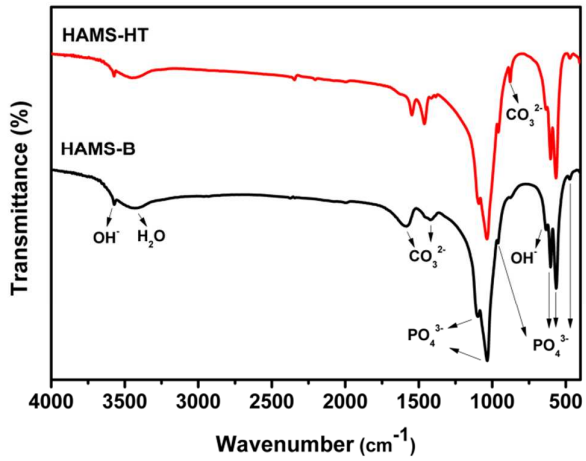

Fig. 4 FTIR spectra of HAMSs.

Table 1 Textural properties and drug loading efficiencies of samples

Samples	S_{BET} (m^2g^{-1})[a]	D (nm)[a]	V (cm^3g^{-1})[a]	L. E. (%)[a]
HAMS-B	79.63	13.75	0.27	-
HAMS-HT	76.03	14.22	0.27	-
HAMS-B-GS200	19.75	7.84	0.04	51.60
HAMS-B-GS500	16.78	6.55	0.03	86.74
HAMS-HT-GS200	16.87	9.39	0.04	70.86
HAMS-HT-GS500	18.40	8.90	0.04	79.63

[a] SBET, D, V and L. E. represent surface area, pore size, pore volume and loading efficiency, respectively.

samples was further demonstrated by the N_2 adsorption-desorption isotherms and the corresponding pore distribution cures (Fig. 5). According to the International Union of Pure and Applied Chemistry (IUPAC), the HAMSs can be classified as type H3 hysteresis loops derived from nanoparticle aggregates with slot-shaped pores,[46] which was consistent with the SEM observation (Figs. 1c and d). The isotherm curve of the HAMSs showed a steep increase between 0.9 and 1.0 of P/P_0, indicating the presence of macropores.[29] While a great majority of pore volume was contributed by mesopores, as shown in Fig. 5b, most of the pores were 2-50 nm in size. Based on the desorption branch of the nitrogen isotherm, as caculated with the BJH method, the average pore sizes of HAMS-B and HAMS-HT samples were determined to be 13.75 and 14.22 nm, respectively. When compared with the HAMS-B samples, the HAMS-HT samples had similar BET specific surfaces area and pore volumes (Table 1).

3.2 Cell viability

Live/dead staining was used to observe cell viability after culturing the mBMSCs on the HAMSs for 3 d. The calcein AM produces an intense uniform green fluorescence in live cells, while PI produces a bright red fluorescence in dead cells. As shown in Figs. 6a-e, a vast majority of cells exhibited good

RSC Advances

PAPER

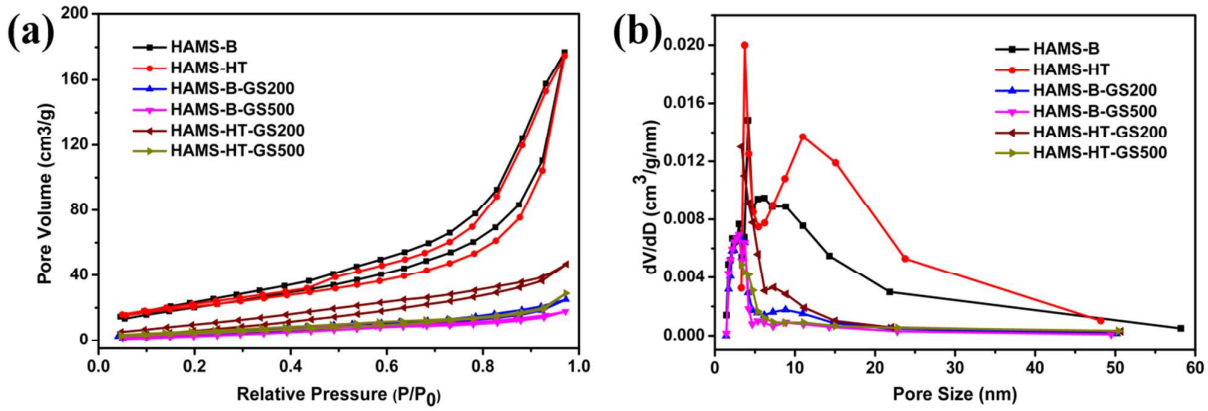

Fig. 5 Nitrogen adsorption-desorption isotherms (a) and pore size distribution (b) of HAMS-B, HAMS-HT, HAMS-B-GS200, HAMS-B-GS500, HAMS-HT-GS200 and HAMS-HT-GS500.

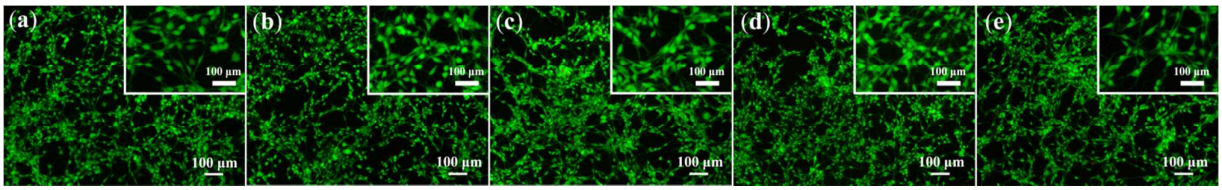

Fig. 6 Live/dead staining results of mBMSCs co-culturing 3 d with HAMS particles in different concentration were shown as: (a) 0 μg mL^{-1}, (b) 100 μg mL^{-1} HAMS-B, (c) 200 μg mL^{-1} HAMS-B, (d) 100 μg mL^{-1} HAMS-HT, (e) 200 μg mL^{-1} HAMS-HT. The medium without samples served as the positive control.

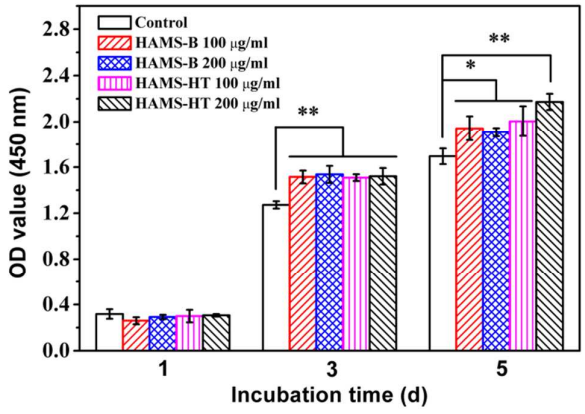

Fig. 7 CCK-8 assay results of mBMSCs co-culturing 1, 3 and 5 d with HAMS particles at different concentrations. The data were represented as the means ± SD, n=4; differences were considered significant when *P < 0.05, **P < 0.01.

viability. Moreover, most mBMSCs had numerous pseudopodia and were spindle-shaped, indicating excellent physiological status of cells (the inset in Figs. 6a-e).

The HAMS-B and HAMS-HT-treated mBMSC samples were subjected to cytotoxicity studies at different dosages; the results are shown in Fig. 7. None of the HAMS concentrations tested had a significant effect on cell viability when compared with the control cells at a culture time of 1 d. Up to 3 and 5 d, the cells displayed significantly higher proliferation ability on HAMS-B and HAMS-HT compared with the control. These results demonstrated that the cells presented stable proliferation ability on all HAMSs as the culture time increased. Prior studies have demonstrated that low concentrations of Ca^{2+} were suitable for the proliferation and survival of the cells.[47] Therefore, the increase in cell viability observed after 3 and 5 d of culture for the concentrations of 100 and 200 μg mL^{-1} could be attributed to the release of Ca^{2+} from the HAMSs. The in vitro cell assay results demonstrated that the HAMSs have excellent in vitro biocompatibility and can stimulate the proliferation of the mBMSCs.

3.3 *In vitro* drug release properties of HAMSs

To investigate the capability of HAMSs as drug carriers, GS was introduced into the pores of HAMSs. As shown in Fig. 5, the hystereses in the middle sections of desorption isotherms and the peaks in the pore size distribution curves were weakened after GS loading. The BET specific surface area (S_{BET}) and pore volume (V_P), respectively, decreased from 79.63 m^2/g and 0.27 cm^3/g for HAMS-B to 19.75 m^2/g and 0.04 cm^3/g for HAMS-B-GS200 and 16.78 m^2/g and 0.03 cm^3/g for HAMS-B-GS500. When compared with the HAMS-B delivery systems, the S_{BET} and V_P decreased from 76.03 m^2/g and 0.27 cm^3/g for HAMS-HT to 16.87 m^2/g and 0.04 cm^3/g for HAMS-HT-GS200 and 18.40 m^2/g and 0.04 cm^3/g for HAMS-HT-GS500 (Table 1). These results indicated that a majority of the pores had been filed after GS loading into the HAMSs.

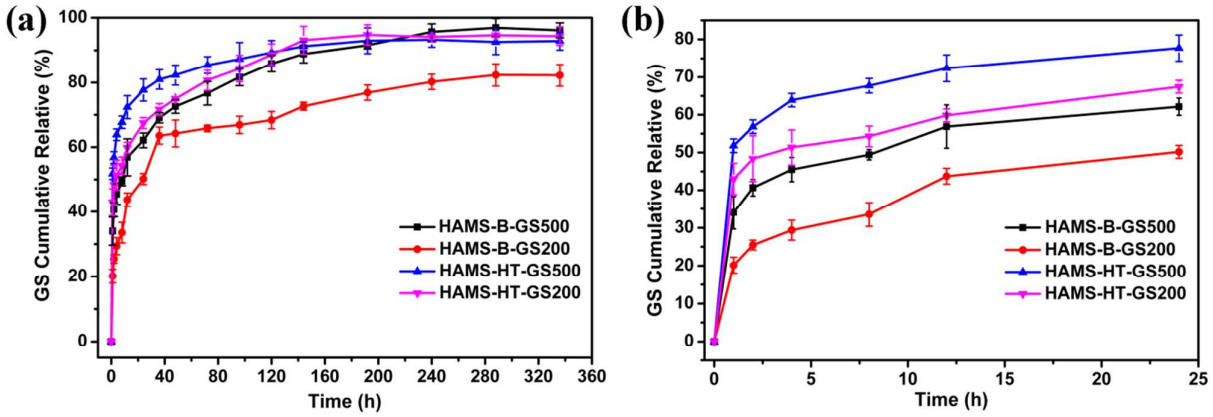

Fig. 8 The *in vitro* GS release profile of samples in PBS for 336 h (a) and 24 h (b).

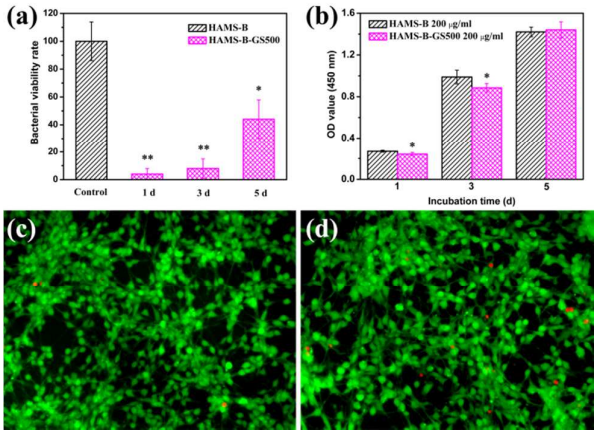

Fig. 9 (a) The antimicrobial activity (n=4) of HAMS-B-GS500 after 1, 3 and 5 d of GS release. (b) CCK-8 assay (n=4) results of mBMSCs co-culturing 1, 3 and 5 d with samples. Live/dead staining of mBMSCs after co-culturing with HAMS-B (c) and HAMS-B-GS500 (d) for 3 d. ** denotes $P < 0.01$, and * denotes $P < 0.05$ compared with HAMS-B sample.

As shown in Table 1, the HAMS-GS500 system exhibited a significantly higher drug loading efficiency (79.63% to 86.74%) than that of the HAMS-GS200 syetem (51.60% to 70.86%). The good drug loading efficiencies of the HAMSs may be attributed to the high specific surface area and pore volume. The numerous HA nanorods or nano-needles on the microsphere surfaces aggregated to form mesopores or macropores, ideal for drug-transferring channels, and also improved the surface areas for increased GS loading (Figs. 1c and d).

The drug-release profiles of the HAMS-GS delivery systems in PBS are shown in Fig. 8. The release rates of GS from the HAMS-HT system were significantly higher than that of the HAMS-B system with varying drug-loading concentrations in the first 24 h (Fig. 8b). For the HAMS-B-GS200 system, 82% of GS were released over a prolonged period of 336 h. For the HAMS-B-GS500 system, the drug release was nearly complete within 288 h (Fig. 8a). These two drug delivery systems exhibited slow and sustained releases of GS, which could be applicable when controlled release is desired, e.g., in long-term healing applications. However, in the first 24 h, the HAMS-HT-GS500 and HAMS-HT-GS200 systems initially displayed rapid GS release rates of 78% and 67%, respectively (Fig. 8b). These profiles would be applicable when high dosages are required immediately after surgery.

The release curves can be divided into two patterns: an initial fast release followed by a slow release. The drug release behaviour of the HAMSs may be due to the types of GS adsorption into or onto the microspheres, i.e., physical or

chemical adsorptions.[48] In the initial release period of HAMS-GS in PBS, the rapid drug release was primarily caused by the external physical adsorption of GS molecules to the surfaces and macropores of the HAMSs. Furthermore, previous studies have demonstrated that drug molecules contain hydroxyl and amino groups interact with the Si-OH and P-OH groups of drug carriers though hydrogen bonding, i.e., chemical adsorption.[49-52] Therefore, the slow release profiles may be attributed to the hydrogen bonding between the P-OH moieties in the HAMSs and the hydroxyl and amino groups in the GS molecules.

3.4 Antibacterial activity

GS is a concentration-dependent aminoglycoside antibiotic,[53] and thus, a high concentration of GS is required at the bone-implant interface for the deracination of bacterial infections. In this work, the cell viability results demonstrated that the HAMS-B system had excellent in vitro biocompatibility and could stimulate the proliferation of mBMSCs. Moreover, the HAMS-B-GS500 system exhibited a much higher loading efficiency than the other three systems and also showed a slow and sustained release of GS. Therefore, the HAMS-B-GS500 system was considered appropriate to serve as a controlled antibiotic delivery system for investigating antibacterial activity.

The antibacterial activity and the biocompatibility of the HAMS-B-GS500 system are shown in Fig. 9. When compared with the HAMS-B system, the HAMS-B-GS500 system exhibited excellent inhibition against S. epidermidis. After 1, 3 and 5 d of drug release, the bacterial viability rates of the HAMS-B-GS500 system were approximately 4%, 8% and 44%, respectively (Fig. 9a). An ideal drug delivery system for the treatment of bone infection should possess good drug loading-release, bactericidal properties and excellent biocompatibility. As shown in Fig. 9b, the HAMS-B-GS500 system at a concentration of 200 μg mL^{-1} showed an inhibitory effect on mBMSCs viability when compared with the control cells after 1 and 3 d culture; no significant difference was observed after 5 d. The live/dead assays revealed that the mBMSCs exhibited a well-spread morphology in all samples. Moreover, very few dead cells were present on the HAMS-B and HAMS-B-GS500 systems (Figs. 9c and d). These results demonstrated that the HAMS-B-GS500 system had excellent in vitro biocompatibility, antimicrobial activity and no toxic effects on mBMSCs.

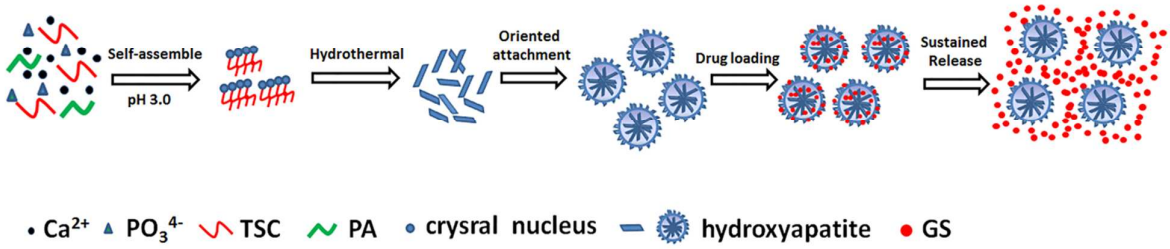

Fig. 10 Scheme for the formation processes of HAMSs and subsequent loading and release of GS molecules.

3.5 Formation and drug release mechanism of HAMSs

The formation of hierarchical nanostructures and drug release processes is proposed in Fig. 10. A Ca^{2+}-chelated TSC initially formed a citrate calcium complex. As stirring time increased, the complex gradually formed nanoparticles and fused with each other to reduce the overall system energy. As the reaction continued, hydrothermal temperature and pressure increased, Subsequently, HA microsheets precipitated and aggregated to form spherical structures to further reduce the overall system energy. Ostwald ripening suggested that large crystallites grew at the expense of smaller crystals.[54] As the

crystal growth continued, the solid hierarchical nanostructured HAMSs were finally obtained. The GS molecules were loaded into the interior or adsorbed onto the surface of HAMSs by physical adsorption and chemical adsorption (responsible for the burst and sustained release profiles, respectively, of GS).

4. Conclusions

In the present study, HAMS particles with hierarchical porous structures developed through hydrothermal treatment using PA as s pH-adjusting agent and TSC as a regulating agent. The well-defined 3D nanostructures constructed by nanoplates as building blocks endowed the products with numerous mesoporous and macroporous channels and high specific areas, which are impotant factors in the design of drug delivery carriers. The HAMSs showed high drug loading efficiencies and good sustained release properties. The viability assays confirmed that all samples promoted the proliferation at 3 and 5 days. The HAMS-B system was economic and time-saving when compared with the HAMS-HT system. Moreover, the HAMS-B-GS500 system exhibited much higher loading efficiency than the other three systems. Additionally, the HAMS-B-GS500 system exhibited excellent antimicrobial activity and good biocompatibility. The present results show the promising potential of HAMSs as a drug carrier for the local delivery of both chemical and biological therapeutic drugs.

Acknowledgements

The authors sincerely thank Professor Xuetao Shi, South China University of Technology, Guangzhou, China, for his kind help on the preparation of this manuscript. This work was financially supported by the National Basic Research Programme of China (Grant No. 2012CB619100), the National Natural Science Foundation of China (Grant No. 51232002), the Science and Technology Programme of Guangdong Province (Grant No. 2012A061100002) and the Fundamental Research Funds for the Central Universities (Grant No. 2015ZZ009).

References

1 D. Dallari, L. Savarino, U. Albisinni, P. Fornasari, A. Ferruzzi and N. Baldini, *Biomaterials*, 2012, **33**, 72-79.
2 B. K. Culpepper, D. S. Morris, P. E. Prevelige and S.L. Bellis, *Biomaterials*, 2013, **34**, 2455-2462.
3 A. Oyane, X. P. Wang, Y. Sogo, A. Ito and H. Tsurushima, *Acta Biomater.*, 2012, **8**, 2034–2046.
4 J. D. Chen, Z. H. Wang, Z. L. Wen, S. Yang, J. H. Wang and Q. Q. Zhang, *Colloids Surf., B*, 2015, **127**, 47-53.
5 P. Yang, Z. Quan, Z. Hou, C. Li, X. Kang and Z. Cheng, *Biomaterials*, 2009, **30**, 4786-4795.
6 W. Zhang, Y. Chai, X. Xu, Y. Wang and N. Cao, *Appl. Surf. Sci.*, 2014, **322**, 71-77.
7 Y. P. Guo, L. H. Guo, Y. B. Yao, C. Q. Ning and Y. J. Guo, *Chem. Commun.*, 2011, **47**, 12215-12217.
8 C. Qi, Y. J. Zhu, B. Q. Lu, X. Y. Zhao, J. Zhao and F. Chen, *Chem. Eur. J.*, 2013, **19**, 5332-5341.
9 H. B. Zhang, K. C. Zhou, Z. Y. Li and S. P. Huang, *J. Phys. Chem. Solids*, 2009, **70**, 243-248
10 Y. J. Guo, Y. Y. Wang, T. Chen, Y. T. Wei, L. F. Chu and Y. P. Guo, *Mater. Sci. Eng. C*, 2013, **33**, 3166-3172.
11 Y. P. Guo, Y. B. Yao, Y. J. Guo and C. Q. Ning, *Microporous Mesoporous Mater.*, 2012, **155**, 245-251.
12 M. Sivakumar, I. Manjubala and K. Panduranga Rao, *Carbohyd. Polym.*, 2002, **49**, 281-288.
13 R. Sun R, Y. Lu Y and K. Chen, *Mater. Sci. Eng., C*, 2009, **29**, 1088-1092.
14 T. J. Wu, H. H. Huang, C. W. Lan, C. H. Lin, F. Y. Hsu and Y. J. Wang, *Biomaterials*, 2004, **25**, 651-658.
15 M. H. Hong, J. S. Son, K. M. Kim, M. Han, D. S. Oh and Y. K. Lee, *J. Mater. Sci. Mater. Med.*, 2011, **22**, 349-355.
16 J. S. Cho and Y. C. Kang, *J. Alloys Compd.*, 2008, **464**, 282-287.
17 Y. Mizushima, T. Ikoma, J. Tanaka, K. Hoshi, T. Ishihara and Y. Ogawa, *J. Controlled Release*, 2006, **110**, 260-265.
18 S. A. Hutchens, R. S. Benson, B. R. Evans, H. M. O'Neill and C. J. Rawn, *Biomaterials*, 2006, **27**, 4661-4670.
19 H. Yang, L. J. Hao, N. R. Zhao, C. Du and Y. J. Wang, *Cryst. Eng. Comm.*, 2013, **15**, 5760-5763.
20 M. Yu, K. C. Zhou, F. J. Zhang and D. Zhang, *Ceram. Int.*, 2014;**40**:12617-12621.
21 C. Takai, T. Hotta, S. Shiozaki, Y. Boonsongrit and H. Abe, *Chem. Commun.*, 2009, **37**, 5533-5535.
22 L. X. Yang, J. J. Yin, L. L. Wang, G. X. Xing, P. Yin and Q. W. Liu Q, *Ceram. Int.*, 2012, **38**, 495-502.
23 R. Kniep and S. Busch. *Angew. Chem. Int. Ed. Engl.*, 1996, **35**, 2624-2626.
24 L. M. Anabel, G. M. Jaime and R. C. Rafael, *Adv. Mater.*, 1998, **10**, 49-53.
25 H. Yang, L. Hao, N. Zhao, M. Huang, C. Du and Y. Wang, *Mater. Chem. Phys.*, 2013, **141**, 488-494.
26 Y. J. Wu and Y. H. Tseng, *Cryst. Growth Des.*, 2010, **10**, 4240-4242.
27 H. Yang, L. J. Hao, C. Du and Y. J. Wang, *RSC Adv.*, 2013, **3**, 23184-23189.
28 L. J. Hao, H. Yang, N. R. Zhao, C. Du and Y. J. Wang, *Powder Technol.* 2014, **253**, 172-177.
29 J. Wu, Y. J. Zhu, S. W. Cao and F. Chen, Adv. Mater., 2010, **22**, 749-753.
30 R. L. Grant, C. Yao, D. Gabaldon and D. Acosta, *Toxicol.*, 1992, **76**, 153-176.
31 M. Aviv, I. Berdicevsky and M. Zilberman, *J. Biomed. Mater. Res. A,* 2007, **83**, 10-19.

32 Y. Liu, Z. Zheng, J. N. Zara, C. Hsu, D. E. Soofer, K. S. Lee, R. K. Siu, L. S. Miller, X. Zhang and D. Carpenter, *Biomaterials*, 2012, **33**, 8745-8756.
33 Y. P. Guo, T. Long, S. Tang, Y. J. Guo and Z. A. Zhu, *J. Mater. Chem. B*, 2014, **2**, 2899-2909.
34 Y. Cai and R. Tang, *J. Mater. Chem.*, 2008, **18**, 3775-3787.
35 M. Virto, P. Frutos, S. Torrado and G. Frutos, *Biomaterials*, 2003, **24**, 79-87.
36 M. R. Virto, B. Elorza, S. Torrado, M. d. L. A. Elorza and G. Frutos, *Biomaterials*, 2007, **28**, 877-885.
37 J. M. Andrews, *J. Antimicrob. Chemother.*, 2001, **48**, 5-16.
38 Y. J. Ma, L. J. Hao, S. L. Du and N. R. Zhao, *J. Inorg. Mater.*, 2014, **29**, 284-288.
39 L. J. Hao, H. Yang, S. L. Du, N. R. Zhao and Y. J. Wang, *Mater. Lett.*, 2014, **131**, 252-254.
40 B. Z. Ristic, M. M. Milenkovic, I. R. Dakic, B. M. Todorovic-Markovic, M. S. Milosavljevic, M. D. Budimir, V. G. Paunovic, M. D. Dramicanin, Z. M. Markovic and V. S. Trajkovic, *Biomaterials*, 2014, **35**, 4428-4435.
41 H. Eimar, E. Ghadimi, B. Marelli, H. Vali, S. N. Nazhat, W. M. Amin, J. Torres, O. Ciobanu, R. F. A. Junior and F. Tamimi, *Acta Biomater.*, 2012, **8**, 3400-3410.
42 M. E. Fleet and X. Liu, *J. Solid State Chem.*, 2003, **174**, 412-417.
43 M. Iafisco, A. Ruffini, A. Adamiano, S. Sprio and A. Tampieri, *Mater. Sci. Eng., C*, 2014, **35**, 212-219.
44 C. Rey, V. Renugopalakrishman, B. Collins and M. J. Glimcher, *Calcified tissue int.*, 1991, **49**, 251-258.
45 T. Long, Y. P. Guo, Y. Z. Liu and Z. A. Zhu, *RSC Adv.*, 2013, **3**, 24169-24176.
46 K. Sing, D. Everett, R. Haul, L. Moscou, R. Pierotti and J. Rouquerol, *Pure Appl. Chem.*, 1985, **57**, 603-619.
47 S. Maeno, Y. Niki, H. Matsumoto, H. Morioka, T. Yatabe, A. Funayama, Y. Toyama, T. Taguchi and J. Tanaka, *Biomaterials*, 2005, **26**, 4847-4855.
48 L. Zhao, X. Yan, X. Zhou, L. Zhou, H. Wang, J. Tang and C. Yu, *Microporous Mesoporous Mater.*, 2008, **109**, 210-215.
49 W. Xia and J. Chang, *J. Controlled Release*, 2006, **110**, 522-530.
50 A. Sousa, K. Souza and E. Sousa, *Acta Biomater.*, 2008, **4**, 671-679.
51 W. Xia, J. Chang, J. Lin and J. Zhu, *Eur. J. Pharm. Biopharm.*, 2008, **69**, 546-552.
52 R. Govindan and E. Girija, *J. Mater. Chem. B*, 2014, **2**, 5468-5477
53 M. K. Lacy, D. P. Nicolau, C. H. Nightingale and R. Quintiliani, *Clin. Infect. Dis.*, 1998, **27**, 23-27.
54 T. Ogino, T. Suzuki and K. Sawada, *Geochim. Cosmochim. Acta*, 1987, **51**, 2757-2767.

Hierarchically nanostructured hydroxyapatite microspheres as drug delivery carrier and their effects on cell viability

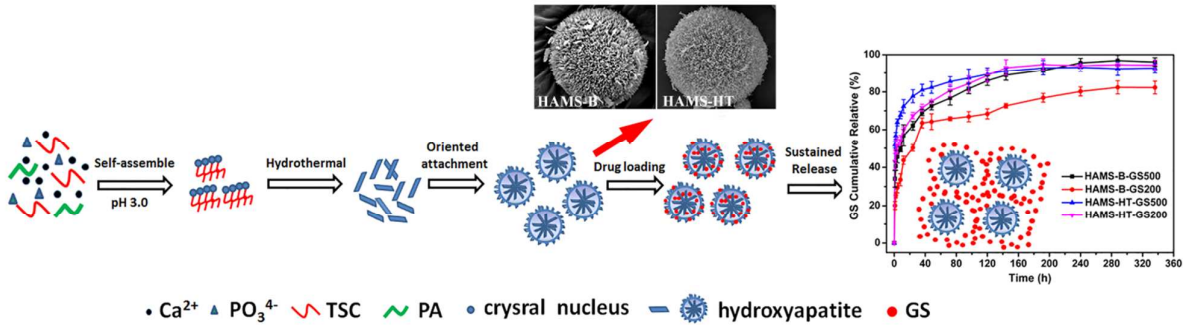

The hydroxyapatite microspheres prepared by hydrothermal synthesis exhibit excellent biocompatibility, high GS-loading efficiency, controllable GS release property and bactericidal property.